RSC Advances

ROYAL SOCIETY OF CHEMISTRY

www.rsc.org/advances

RSC Advances

RSCPublishing

ARTICLE

Controlled growth of Ag nanoparticles decorated onto the surface of SiO_2 spheres: A nanohybrid system with combined SERS and catalytic properties

enCite this: DOI: 10.1039/x0xx00000x

Received ooth January 2014,
Accepted ooth January 2014

DOI: 10.1039/x0xx00000x

www.rsc.org/

L. Tzounis,[a,b] R. Contreras-Caceres,[a,c*] Leonard Schellkopf,[a,b] D. Jehnichen,[a] D. Fischer,[a] Chengzhi Cai,[c] Petra Uhlmann,[a*] Manfred Stamm,[a,b]

A versatile water-based method for depositing silver nanoparticles (Ag NPs) with controllable and uniform metal size onto the surface of silica (SiO_2) spheres is reported. The hybrid particles exhibited a raspberry-like morphology, and their potential for SERS and catalytic applications has been demonstrated. SiO_2 spheres (~120 nm) were synthesized first and modified with polyethyleneimine (PEI) to introduce amine surface functionalities. The amine groups were coordinated with silver ions (Ag^+) and reduced to Ag seeds (~4 nm), uniformly distributed onto the SiO_2 surface (SiO_2@Ag-seed).In order to improve the optical responses and catalytic activity of SiO_2@Ag-seed system, two subsequent silver growth steps were performed. The diameter of Ag seeds was increased to 12 and 19 nm, respectively, hereafter denoted as SiO_2@Ag-1 and SiO_2@Ag-2. The immobilization and controlled growth of Ag NPs was confirmed by UV-vis spectroscopy, scanning and transmission electron microscopy (SEM, TEM). All specimens displayed satisfactory SERS activity increasing with the Ag NP size, showing clear Raman peaks of Rhodamine 6G (R6G) at very low concentration. The SiO_2@Ag particles were also tested and compared for their catalytic efficiency towards the reduction of 4-nitrophenol (4-Nip) by $NaBH_4$. The principal advantages of this study lie on the ability to tune the Ag NP size, the long-term colloidal stability of all fabricated SiO_2@Ag systems in aqueous media, and the limited use of hazardous chemicals and pollutant organic solvents during the synthetic process.

1. Introduction

During the last decades, the synthesis and characterization of noble metal nanoparticles, defined as particles with a diameter between 1 and 100 nm, have attracted an extensive research interest.[1] This can be easily realized due to the fact that at this size level the materials' properties differ remarkably from that at the macroscopic scale.[2] These differences are, amongst others, caused by the well-known localized surface plasmon resonance (LSPR).[3,4] This phenomenon is produced when an external electromagnetic field interacts with a metal nanoparticle resulting in the delocalization of the electron cloud. From that, two important consequences are induced: *i)* an intense absorption band in the UV-vis spectrum, supplying interesting optical properties[5] and *ii)* an increase in the local electromagnetic field near the nanoparticle surface, exploited for surface-enhanced Raman spectroscopy (SERS) applications.[6-8] Nowadays, there is no doubt that metal NPs due to their unique physical and chemical properties are considered as very promising materials in the field of drug delivery, photonics, catalysis, ultrasensitive biosensors via SERS substrates, etc.[9-11] In specific, the SERS effect was discovered by Martin Fleischman in 1974 as a large enhancement of the Raman signal of certain molecules adsorbed on roughened metallic surfaces.[12] From that time, a great number of noble metal nanoparticles have been proposed for SERS ultradetection, including mainly silver, gold and copper. However, silver is by far the most common used plasmonic material, since Ag NPs expose the strongest surface plasmon band.[13] This is attributed to the higher energy of the interband transition (~3.2 eV) relative to the energy of the plasmon resonance, leading to a minimum damping of the plasmon.[14] Noble metal NPs have been several times also reported as catalysts in many electron-transfer chemical reactions. Their high surface area enables a large percentage of atoms from their surfaces to be accessible from the environment's media, and this can explain their excellent catalytic capabilities.[15]

Several methods have been reported for the synthesis of Ag NPs which can be divided into traditional and non-traditional ones.[16] The term 'traditional' is used for solution-phase synthetic protocols based on the reduction of a silver salt. The most common methods were developed by Creighton and Lee who used silver nitrate ($AgNO_3$) as a metal source and sodium borohydride ($NaBH_4$) or sodium citrate as a reducing agent, respectively.[17,18] So far, different silver salts and reducing agents have been used to obtain stable and monodisperse Ag NPs in solution.[19,20] The so called 'non-traditional' methods, include Ag particle synthesis through high-temperature reduction in porous solid matrices,[21] vapor-phase condensation of metal onto a solid support, ablation of a metal target into a suspending liquid,[23] photoreduction of silver ions,[24] and electrolysis of a silver salt

solution.[25] Unfortunately, both of the two approaches have to face some inherent problems. Traditional methods have a limited range in the final size of the particles, producing in most of the cases particles below 10 nm, not sufficient for optical and spectroscopic purposes. On the other hand, the main disadvantages of non-traditional methods are the wide size distribution, lack of crystallinity, high cost, and up-scaling of the fabrication process.

Recently, some strategies have been proposed to overcome the previously mentioned problems related to the traditional synthetic methods. Hybrid systems composed of polymer-nanoparticle or inorganic material-nanoparticle arrangements have been developed, where metal NPs can endow their unique properties to the resulting nanoassemblies. The structure and functionalities of the host material used as the support can control the spatial distribution of nanoparticles. Therefore, the most prominent problem which is the tendency of nanoparticles to agglomerate due to their high surface energy can be avoided.[26] In specific, different organic materials such as dendrimers,[27] latex particles,[28] microgels,[29] polymers brushes,[30, 31]graphene sheets[32], as well as inorganic materials like SiO_2 microspheres[33,34,35] have been utilized as carriers for the immobilization of metal NPs. Liu et al. used poly(amidoamine) (PAMAM) dendrimers to incorporate Ag NPs after the reduction of Ag ions by $NaBH_4$, previously interacted with the branched structure of PAMAM.[27] The disadvantage of this protocol is that the final size of metal NPs is determined by the dimension of the dendrimer, limiting the method only for small particles. Chen et al. synthesized poly(N-isopropylacrylamide)-coated latex microgels, and deposited Ag nanospheres on the microgel surface in an ethanol/water media.[28] The Ag NPs were produced via in situ reduction of Ag^+ by radicals generated from the polymerization initiator. Ballauff et al. used also the same core-shell system to immobilize Ag NPs via chemical reduction of Ag^+ with sodium borohydride. The resulting hybrid system was proposed for catalytic applications tunable with temperature variations.[29] In both cases, non-biocompatible polymers were used preventing from bio-medical applications. Hence, in order to overcome this obstacle, metal coated SiO_2 particles have gained a tremendous interest and many synthetic approaches have been reported.[33,34,35] Deng el al. used polyvinylpyrrolidone (PVP) as reducing and stabilizing agent for the fabrication of SiO_2@Ag nanocomposites.[36] Although no additional reducing agent was required, the synthesis is unfeasible in aqueous media and limited for particles dispersed finally in an organic solvent. Zhu el al. used an electroless process to obtain core-shell SiO_2@Ag submicrometer spheres. In that case, the silica surface was modified with Sn^{2+} ions in a first step, and then reduced by an ammoniacal silver nitrate solution at low concentration in a mixture of ethanol/formaldehyde.[37] Nevertheless, the use of toxic formaldehyde is an important drawback of this protocol. Kobayashi et al. used as well an electroless plating process to deposit Ag NPs on silica spheres. Initially, they modified the silica surface with $SnCl_2$, and then Ag^+ where reduced toAg^0, while Sn^{2+} oxidizes to Sn^{4+}, leading to a homogeneous deposition of Ag NPs.[38] However, in order to obtain a relatively dense Ag coating, the two step process had to be repeated several times. One protocol which has shown a very simple and scalable process to deposit silver or gold nanoparticles onto the surface of silica spheres has been reported by Tian el al.[34] Polyethyleneimine was used as a cationic polyelectrolyte to modify the silica surfaces, and subsequently acted as the linker of metal ions as well as the reducing agent. A great motivation could be given from this study to our synthetic process; however, practical uses of the hybrid silica/Ag particles have not been elucidated.

Herein, a versatile and low-toxicity synthetic approach is proposed for the successful decoration of SiO_2 spheres with monodisperse Ag NPs of variable size. The hybrid SiO_2@Ag particles exhibited a raspberry-like morphology which is believed to endow the long-term colloidal stability to our systems. Furthermore, the controlled growth of Ag NPs facilitates the enhancement of the optical and catalytic properties with a promising performance as compared to existing systems from the literature. In a first step, silica particles were synthesized through the well-known Stöber method,[39] and treated with polyethyleneimine to promote amine surface functionalities. Silver cations, supplied by $AgNO_3$ aqueous solution, interacted with the amine groups by means of coordinative interactions, and reduced to metallic Ag seed particles by $NaBH_4$. This process resulted in spherical Ag NPs with a uniform size of about 4 nm immobilized onto the silica surface (SiO_2@Ag-seed). After that, two subsequent Ag growth steps were carried out to increase the Ag NP size in a controlled manner. Throughout this strategy, Ag NPs with 12 nm (SiO_2@Ag-1) and 19 nm (SiO_2@Ag-2) average size were generated. FT-IR and electrokinetic analysis confirmed the presence of amine groups on the silica spheres. SEM and TEM images demonstrated the successful decoration of Ag NPs onto the silica spheres, as well as the increase of Ag NP size. UV-vis spectroscopy proved the optical responses of the hybrid systems, and verified the Ag growth by the relative shift of the maximum plasmon resonance band. SERS studies using Rhodamine 6G as a model analyte molecule revealed that SERS activity improved with the increased Ag NP size. SERS investigations clearly suggest the potential use of all fabricated SiO_2@Ag nanocolloids for the determination of active SERS molecules such as pesticides, contaminants or other water pollutants at very low concentrations. The catalytic activity of SiO_2@Ag systems was highlighted by the reduction of 4-nitrophenol (4-Nip) to 4-aminophenol (4-Amp) in the presence of sodium borohydride ($NaBH_4$), and it was found to be increased also with the increase of Ag NPs size. The excellent catalytic and SERS performance of all the systems presented here suggest that they could be ideal candidates for biomedical applications, water treatment, heterogeneous catalysis and ultrasensitive detection via SERS substrates.

2. Experimental

2.1. Materials

Tetraethyl orthosilicate (TEOS, 97%), ammonium hydroxide (28%), absolute ethanol (99.5%), silver nitrate ($AgNO_3$, ≥99.0%), sodium borohydride ($NaHB_4$), polyethyleneimine (PEI) of low molecular weight (M_n=600 g/mol), cetyltrimethylammonium bromide (CTAB), glycine (≥98.5%) and L-ascorbic acid were purchased from Sigma-Aldrich. Sodium hydroxide, Rhodamine 6G and 4-nitrophenol (4-$C_6H_5NO_3$) were supplied by Fluka. All chemicals were ACS grade and used as received without further purification. Water was purified using a Milli-Q system (Millipore), hereafter referred to as MilliQ water, and used throughout all the preparation and cleaning steps.

2.2. Synthesis of silica spheres (~120 nm)

Prior to use, all glassware were cleaned with a 3:1 v/v acidic solution consisting of hydrochloric/nitric acid (36% and 68%, respectively) and then rinsed copiously with MilliQ water. Monodisperse SiO_2 spheres were synthesized through base-catalyzed hydrolysis of TEOS following the protocol of An et al. with some slight modifications.[40] In brief, a round bottom flask was charged

with 3.3 mL of saturated ammonia solution (28%) and 47 mL of ethanol under magnetic stirring to form a homogeneous solution. In this mixture, 4 mL of TEOS were injected and kept under stirring at 750 rpm for 24 h. The resulting SiO_2 spheres were centrifuged, washed with ethanol and dried under vacuum at 50 °C for 24 h. The washing steps with centrifugation and redispersion in ethanol were repeated at least five times in order to fully purify the particles.

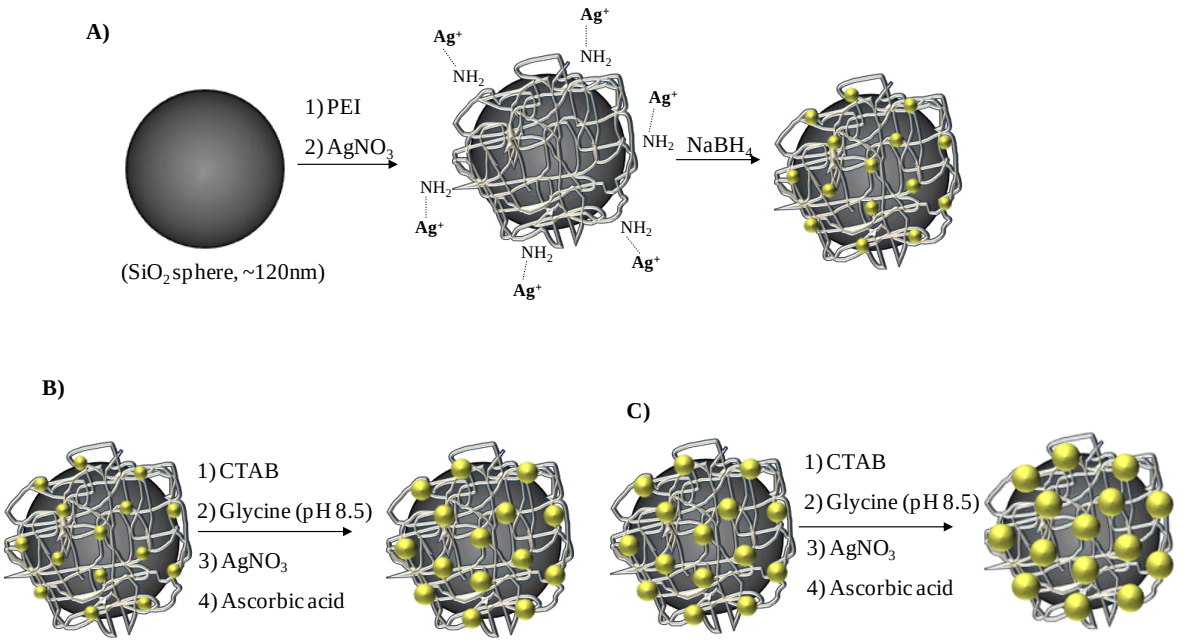

Scheme 1. A) Schematic illustration for the decoration of silica spheres with silver seeds using PEI as ligand of silver ions, and further silver growth on the preformed silver seeds using two subsequent growth steps (B and C).

2.3. Decoration of SiO_2 spheres with Ag seeds (SiO_2@Ag-seed)

Initially, 100 mg of SiO_2 spheres were dispersed in 100 mL of MilliQ water and sonicated for 30 min to fully disperse them. To this colloidal solution, 5 mL of PEI aqueous solution (2 mg/mL) were added under gentle magnetic stirring. The mixture was kept for 30 minutes to achieve the adsorption of positively charged PEI chains onto the negatively charged SiO_2 surface, followed by centrifugation at 8000 rpm for 30 min to remove the excess of PEI. After centrifugation, the supernatant was discarded and the pellet was annealed at 100 °C for 30 min. Afterwards, the PEI modified particles were redispersed in 40 mL of MilliQ water. To this suspension, 1.75 mL of $AgNO_3$ (10 mM) were added dropwise under magnetic stirring and maintained for 30 min to allow a homogeneous coordination of the silver ions with the amine surface moieties. It should be noted that the amine groups are capable of forming complexes with metal ions via coordination.[41] The resulting mixture was centrifuged at 8000 rpm for 30 min and the precipitate was redispersed in 40 mL of MilliQ water. Finally, 1.75 mL of ice-cold freshly prepared $NaBH_4$ solution (50 mM) as a strong reducing agent was added under vigorous stirring to promote the Ag NP growth. Simultaneously, a rapid color change to slight yellow was observed indicating the formation of Ag NPs (seeds). The stirring was slowed down after 30 min to ensure that complete reduction has occurred. The solution was centrifuged then at 8000 rpm for 45 min, followed by removal of the supernatant and redispersion in 40 mL of MilliQ water. Subsequent centrifugation-redispersion steps were conducted to remove traces of $NaBH_4$ as well as Ag NPs not strongly bound to the SiO_2 surface. Finally, the SiO_2@Ag-seed particles were dispersed and remained in 100 mL of MilliQ water. The average size of Agseeds was statistically extracted from the TEM images and found to be (4.2 ± 1.1) nm. The procedure described above is illustrated schematically in Scheme 1A.

2.4. Silver growth using SiO_2@Ag-seed particles

As mentioned in the introduction, two subsequent silver growth steps were performed over theSiO_2@Ag-seed system, using a slightly modified protocol of Yang et al.[42] In detail, for the preparation of the SiO_2@Ag-1 system, 5 mL of a solution composed by 0.4 M glycine buffer solution with pH 8.5 (adjusted by addition of NaOH, 1 M) and CTAB (200 mM) were mixed with 5 mL SiO_2@Ag-seed particles. Then, 100 μL of $AgNO_3$ (10 mM) were added under medium magnetic stirring. After 30 min, 50μL of ascorbic acid (50 mM) as a mild reducing agent were added under vigorous magnetic stirring. The mixture was maintained under stirring for 30 min, followed by centrifugation (8000 rpm, 30 min). The supernatant was removed and the pellet was redispersed in 10 mL of MilliQ water. The average size of Ag NPs after this step was measured by TEM and found to be (12.8 ± 3.4) nm. Further, a second growth step was performed using the previously fabricated SiO_2@Ag-1 particles as seed system. Briefly, 5 mL of a buffer solution composed by 0.4 M glycine at pH 8.5 and CTAB (200 mM) as stabilizer were mixed with 5 mL of SiO_2@Ag-1 particles. Afterwards, 100μL of $AgNO_3$ (10 mM) were added under medium magnetic stirring. After 30 min, the silver reduction was accomplished adding 50μL of ascorbic acid (50 mM) under vigorous magnetic stirring for 30 min. In order to remove excess of ascorbic acid, the solution was centrifuged at 8000 rpm for 30 min, the supernatant was discarded, and the precipitant was redispersed in 10 mL of MilliQ water. TEM analysis revealed an average diameter of Ag NPs in the range of (19.6 ± 3.9) nm. The two silver growth steps yielding SiO_2@Ag-1 and SiO_2@Ag-2 particles exhibiting a

raspberry-like morphology are presented in scheme 1B and 1C, respectively.

2.5. Characterization

Fourier-transformed infrared (FT-IR) spectra were recorded using a Vertex 80v FT-IR spectrometer (Bruker Germany) equipped with a DTGS detector. All the spectra were acquired by signal averaging of 256 scans. Approximately 1.0 mg of neat or PEI modified SiO_2 particles were pressed together with 100 mg of crystalline KBr to form pellets. The zeta-potential of SiO_2 particles as a function of pH was investigated by electrokinetic analysis (EKA) at 25.0 ± 0.2 °C using a zeta potential analyser (Zetasizer Nano-ZS, Malvern Instruments Ltd, UK). Aqueous suspensions with 1.0×10^{-3} M KCl at different pH values were used for the zeta potential determination. The relation between zeta potential and pH was used to determine the isoelectric point (IEP). X-ray diffractometry (XRD) was performed with an X-ray diffractometer XRD T/T (GE Inspection Technologies Ahrensburg, Germany) in symmetric step-scan mode with $\Delta2\Theta = 0.05°$ in transmission mode. The diffractometer operated at 40 kV and 30 mA with Cu Kα radiation. UV-vis spectra were recorded using a Cary 50 scanning spectrophotometer (Varian, USA) with an incorporated xenon flash lamp by using 1-cm quartz cell. Scanning electron microscopy (SEM) was performed using the NEON 40 (Carl Zeiss AG, Germany) scanning electron microscope under an accelerating voltage of 1.0 kV. Samples were prepared by drop casting 100 μL of aqueous suspensions on a 2×1 cm^2 silicon substrate, followed by drying at room temperature in a fume hood. TEM investigations were performed with the Libra 200 transmission electron microscope (Carl Zeiss AG, Germany) operating at 200 kV. Samples for TEM were prepared by dispensing 10 μL of each suspension on a Cu grid with a carbon support membrane. Raman and surface enhanced Raman scattering spectra were measured using the confocal Raman Microscope (CRM) alpha 300R, (WITEc GmbH, Germany). The spectrograph uses high resolution gratings with additional band-pass filter optics and a 2D-CCD camera. Raman and SERS signals were recorded by exciting the samples with a laser power of 5 mW using a laser line (Nd:YAG) at 532 nm. All measurements were obtained in backscattering geometry using a 20× microscope objective with NA values of 0.46 which provided scattering areas of 1.0 μm^2. For one measurement, between 50 and 200 single Raman spectra with a measuring time of 0.5 s were accumulated and the corresponding spectra were recorded within the range of 150-3500 cm^{-1} for Raman shift. For SERS experiments, 1.5 mg of SiO_2@Ag-seed, SiO_2@Ag-1 and SiO_2@Ag-2 particles, respectively, were added into 1.5 mL of Rhodamine (R6G) aqueous solution at a concentration of 10^{-5} M. The solutions were sonicated for 5 min and kept in the dark for half an hour, time enough to reach a thermodynamic equilibrium. A homogenous film of each of the as-prepared SiO_2@Ag/R6G solutions was formed onto the surface of cleaned glass slides by dip coating. Then, the substrates were air-dried and used for the SERS investigations.

2.6. Catalytic reduction of 4-nitrophenol

The catalytic activity was proven quantitatively using a model reaction; the reduction of 4-nitrophenol (4-Nip) to 4-aminophenol (4-Amp) in an excess amount of $NaBH_4$. In a typical experiment, 0.5 mL of freshly prepared $NaBH_4$ (60 mM)aqueous solution was mixed with 2.0 mL of 4-nitrophenol aqueous solution (0.1 mM) in a standard quartz cuvette (path length 1 cm). To this mixture, a constant amount (2 mg) of each of the SiO_2@Ag particles dispersed in 0.2 mL of water was added, and the reaction mixture was monitored immediately by successive UV-vis spectra taken every 50 s in the range of 250-550 nm. All experiments were performed at room temperature (20 °C). The rate constants of the catalytically activated reactions were determined by measuring the change of the peak intensity at 400 nm with time.

3. Results and discussion

3.1. Fourier transformed infrared spectroscopy (FT-IR)

The surface modification of silica spheres with PEI chains was proven in a first instance by FT-IR spectroscopy. Figure 1A shows the FT-IR spectra of SiO_2 particles in the spectra range of 4000-1400 cm^{-1}. For the bare SiO_2 (black dashed line), the broad band at around 3325 cm^{-1} is assigned to the asymmetric stretching vibrations of silanol groups (Si-OH) and adsorbed water molecules, while that at 1631 cm^{-1} belongs to H-O-H bending.[43] In the case of PEI modified particles (red solid line), the band at 3325 cm^{-1} is slightly weakened and new bands appear at 2982 and 2906 cm^{-1} corresponding to the symmetric and asymmetric stretching vibrations of C-H bond, confirming thus the existence of -CH_2 groups. Figure 1B depicts the selected FT-IR spectra region from 1500 to 1350 cm^{-1}, where the peaks located at 1485, 1451 and 1398 cm^{-1} belong to the C-H bending vibrations of the -CH_2 groups arising from the adsorbed PEI molecules.[44] Unfortunately, N-H peaks of the PEI amine groups were overlapped from the band of silanol groups of the SiO_2. However, we can confirm the presence of amine groups with the peak located at 1360 cm^{-1}, corresponding to the C-N stretching vibration.[45]

3.2. Zeta potential measurements

Figure 2 represents the change in zeta potential as a function of pH for bare and PEI functionalized SiO_2 particles at constant ionic strength (10^{-3} M KCl). For the neat SiO_2 particles, the mean zeta potential values are negative in the pH range between 3.0 and 10.0. The isoelectric point (IEP) was found to be slightly below pH 3.0 suggesting a negative surface charge. This could be attributed to the acidic behaviour of the surface silanol groups. On the other hand, for the PEI modified particles, the effect of basic amine groups can explain the positive zeta potential values throughout the pH range between 3.0 and 8.0, while the IEP was slightly below pH 9.0.[46]The results demonstrate an apparent change of the surface charge upon adsorption of the PEI molecules, confirming a successful surface modification.

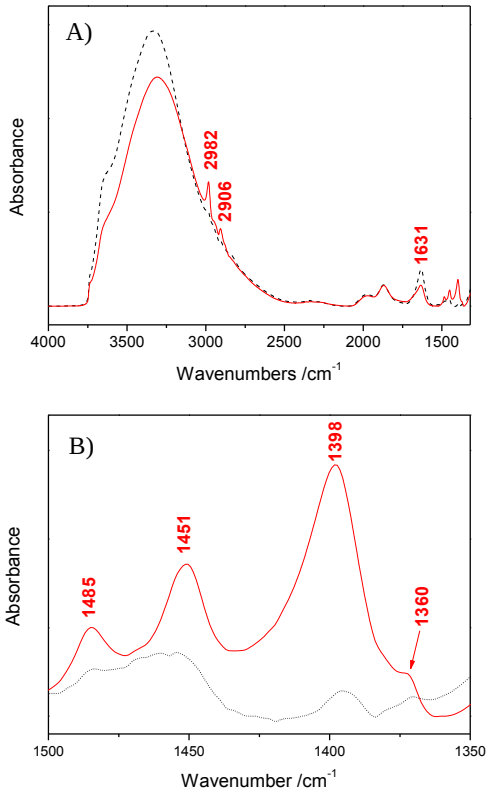

Figure 1. FT-IR spectra of bare SiO_2 (black dashed line) and PEI functionalized SiO_2 particles (red solid line) for A) the spectral region between 4000-1400 cm^{-1} and B) from 1500 to 1350 cm^{-1}.

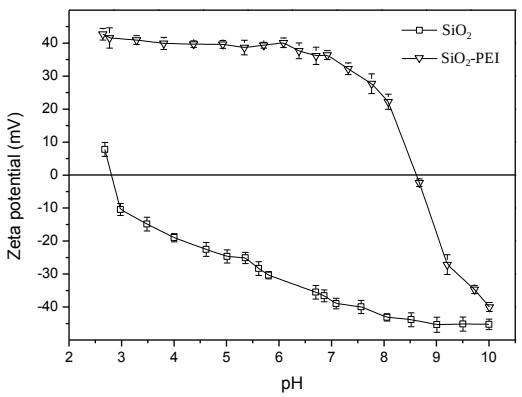

Figure 2. Mean zeta potential as a function of pH for bare and PEI functionalized SiO_2 particles.

3.3. UV-vis spectroscopy of SiO_2 and SiO_2@Ag particles

Figure 3 shows the UV-vis spectra of the three different SiO_2@Ag colloidal systems in aqueous media, as well as for the bare SiO_2 particles at a concentration of 1 mg/mL. The optical image given as an inset demonstrates the high colloidal stability of the suspensions at a concentration of 1 mg/mL, one week after the dispersions have been prepared. It can be observed that the colour changes after immobilization of Ag NPs on the SiO_2 spheres, and especially becomes more intense yellow with the increased Ag NP size. As it was expected, no distinct plasmon band was detected for the SiO_2 spheres. However, after decoration with Ag NPs, each spectrum depicted a localized surface plasmon resonance (LSPR) band with a maximum centered at ca. 400 nm. The presence of a minimum at ca. 320 nm can be also observed, characteristic of the interband transition in the metal that damps the plasmon oscillation in this spectral region.[3] With the increased silver size, the position of the absorption peak is slightly shifted to higher wavelengths. This red-shift is accompanied also by a strong increase in the peak intensity. This behaviour is due to two different factors, *i)* the higher excitation cross-section of the metal nanoparticle in each growth step, and *ii)* the increase of the particle volume.[47] This evolution confirms not only the presence of Ag NPs stabilized onto the SiO_2spheres, but also the increase of particle size during the silver growth steps.

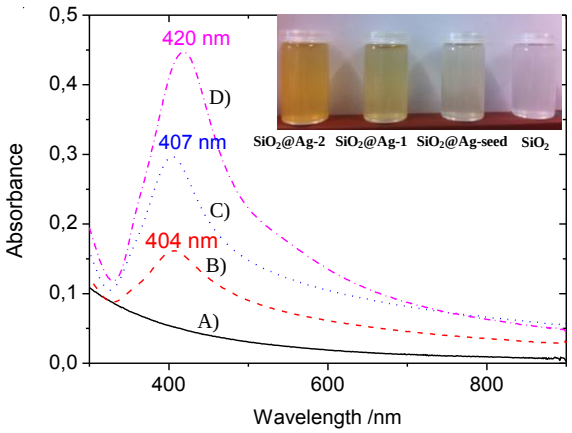

Figure 3. UV-vis spectra of the different colloidal systems in aqueous media: A) bare silica (black solid line), B) SiO_2@Ag-seed (red dashed line), C) SiO_2@Ag-1 (blue dotted line) and D) SiO_2@Ag-2 (pink dashed-dotted line). The optical image given as an inset depicts the high colloidal stability of SiO_2 and SiO_2@Ag systems as well as the changes in colour upon deposition of Ag NPs.

3.4. XRD of SiO_2@Ag nanohybrids

Figure 4 represents a typical X-ray diffraction pattern of the nanohybrid SiO_2@Ag system (pattern of the SiO_2@Ag-2 sample). Sharp diffraction peaks were observed which can be indexed to the face-centered cubic (fcc) structure of metallic Ag (blue lines in Figure 4), with the diffraction peaks corresponding to the (1 1 1), (2 0 0), (2 2 0) and (3 1 1) planes indicating the formation of pure silver of high crystallinity (JCPDS file, No. 4-783). We can also observe the X-ray diffraction of the silica spheres with a broad scattering maximum centered at 22.5º, typical for amorphous SiO_2.[48]

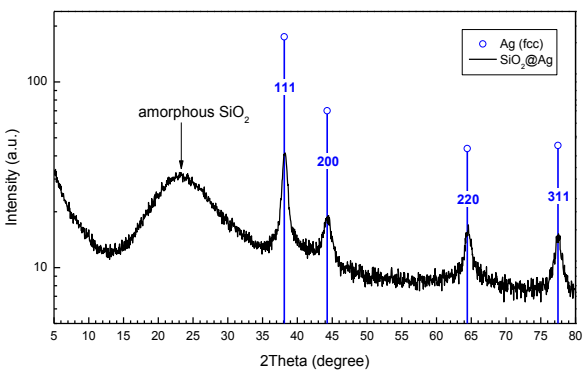

Figure 4. Typical X-ray diffraction pattern of the SiO_2@Ag particles. The blue lines correspond to the pure crystalline Ag diffraction peaks.

3.5. Electron microscopy investigations

The presence of Ag seeds on the SiO_2spheres, as well as the increase of Ag size during the different growth steps were visualized with SEM and TEM images. The representative SEM (left side) and TEM (right side) micrographs of SiO_2 and SiO_2@Ag particles with a raspberry-like morphology, are depicted in Figure 5. Bare SiO_2 particles with uniform size are shown in Figure 5A. Figure 5B demonstrates the morphology of SiO_2@Ag-seed particles, while 5C and 5D represent the SiO_2@Ag-1 and SiO_2@Ag-2 system, respectively. It is important to note that both SEM and TEM investigations reveal no residual silver dots after the silver growth steps, confirming a homogeneous nucleation of Ag NPs. The size of Ag NPs for each of the SiO_2@Ag systems was determined from the corresponding TEM images, and the resulting histograms are plotted in Figure 6. Figure 6A displays the histograms of around 100 NPs analysed for the SiO_2@Ag-seed system, showing an average diameter of (4.2 ± 1.1) nm. The histograms corresponding to the SiO_2@Ag-1 and SiO_2@Ag-2 system are depicted in Figure 6B and 6C, demonstrating a clear increase of the Ag NP size with (12.8 ± 3.4) and (19.6 ± 3.9) nm, respectively.

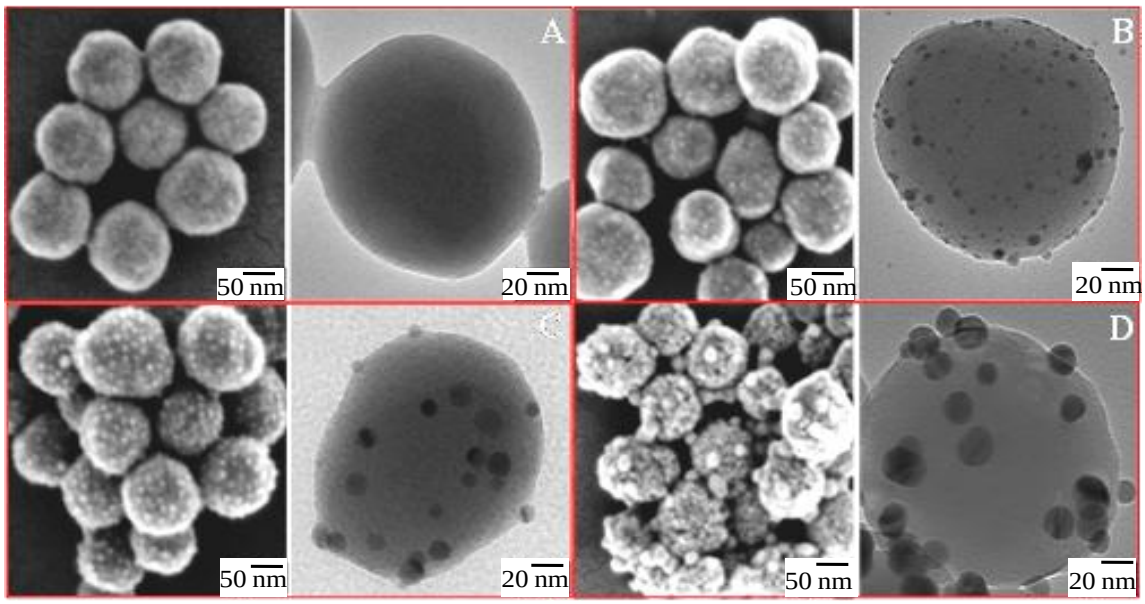

Figure 5. SEM (left side) and TEM (right side) images of A) bare SiO_2, B) SiO_2@Ag-seed, C) SiO_2@Ag-1 and D) SiO_2@Ag-2 hybrid particles exhibiting a raspberry-like morphology.

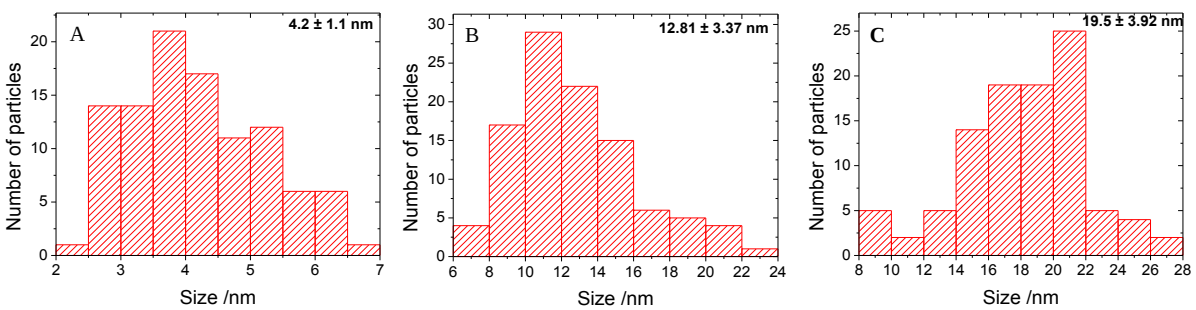

Figure 6. Histogram of 100 Ag NPs measured by TEM images of A) SiO_2@Ag-seed, B) SiO_2@Ag-1 and C) SiO_2@Ag-2 systems, showing the corresponding average size and size distribution.

3.6. SERS experiments

In order to exploit the excellent SERS capabilities of Ag NPs, Rhodamine 6G (R6G) was used as a model analyte to demonstrate the potential of our nanohybrid systems for SERS ultradetection. Figure 7 illustrates the 532 nm excitation SERS spectra of R6G (1.0×10^{-5} M), previously mixed with the three different colloidal suspensions and deposited onto glass slides. It is obvious that all specimens exposed SERS activity as revealed by the characteristic peaks of R6G at 615, 779, 1189, 1316, 1365, 1510, 1577 and 1652 cm^{-1}within the spectral region of 500 to 1800 cm^{-1}, perfectly matching with those found in literature.[49] In addition, the Raman peak located at 1365 cm^{-1} confirms that the enhancement of the

SERS signal increases with the Ag NP size, being in a good agreement with previously reported results.[50, 51] It is important to note that the improvement of the SERS intensity for the SiO_2@Ag-1 and SiO_2@Ag-2 systems is not only attributed to the increased Ag NP size. It is a well-known fact that the SERS property remarkably increases when NPs are close enough to induce coupling between their oscillating surface plasmon. This plasmon coupling is expected only for core-core distances below one particle diameter and produces high local excitation fields.[52] Within SEF=$(I_{surf}/C_{surf})/(I_{bulk}/C_{bulk})$,[30] where I_{surf} and I_{bulk} denote the intensities of the R6G at 1365 cm^{-1} adsorbed to the SiO_2@Ag systems and those of dissolved as bulk in solution (10^{-1}M), respectively. The C_{surf} and C_{bulk} represent the concentrations of R6G used for the Raman and the SERS experiments, respectively. The I_{surf} values at 1365 cm^{-1} (vibration of aromatic C-C stretching band) for the three different systems are provided by the SERS spectra in Figure 7 which correspond to 7211, 14393 and 21897 counts for the SiO_2@Ag-seed, SiO_2@Ag-1 and SiO_2@Ag-2 systems, respectively. Unfortunately, due to the fact that R6G is a fluorescent molecule which absorbs strongly with a maximum at 528 nm, close to the laser measurements (532 nm), no proper value can be assigned to the Raman signal I_{bulk}. Therefore, we assume a maximum value of I_{bulk} in the rage of the detector noise of 200 counts.[30] For the C_{bulk} and C_{surf} values representing the concentrations of R6G solutions used for the Raman and SERS experiments, we used 1.0×10^{-1} M and 1.0×10^{-5} M, respectively. Consequently, the calculated SEFs for the SiO_2@Ag-seed, SiO_2@Ag-1 and SiO_2@Ag-2 are 3.61×10^5, 7.19×10^5 and 1.09×10^6, confirming the relationship between the SERS intensity and the Ag NP size deposited to the SiO_2 surface. The excellent SERS performance of all fabricated systems in combination with their high colloidal stability could be an important parameter for the detection of various water-soluble contaminants by means of SERS spectroscopy.

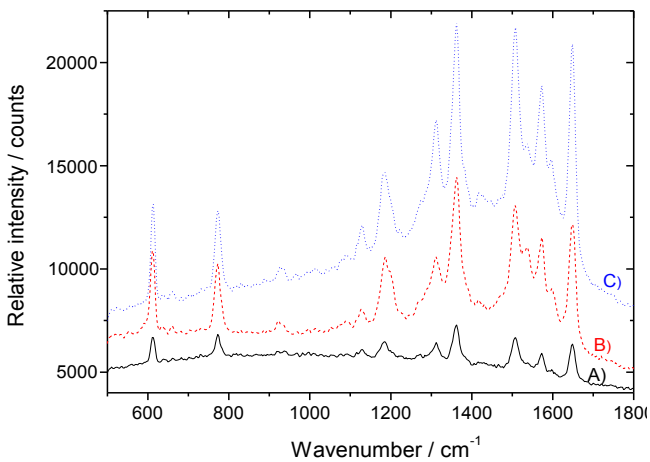

Figure 7. SERS spectra of R6G (10^{-5} M) adsorbed from aqueous solution at the three different samples tested; A) SiO2@Ag-seed (black solid line), B) SiO2@Ag-1 (red dashed line) and C) SiO2@Ag-2 (blue dotted line).

3.7. Catalytic reduction of 4-nitrophenol to 4-aminophenol

The reduction of 4-nitrophenol (4-Nip) to 4-aminophenol (4-Amp) with an excess amount of $NaBH_4$, was employed as a reliable model reaction to evaluate quantitatively the catalytic efficiency of the SiO_2@Ag systems prepared in this work.[53] Although the reduction of 4-Nip to 4-Amp using $NaBH_4$ is thermodynamically favourable (E_0 for 4-Nip/4-Amp= −0.76 V and H_3BO_3/BH_4^- = −1.33 V versus NHE: normal hydrogen electrode), the presence of a kinetic barrier due to the large potential difference between donor and acceptor molecules decreases the feasibility of this reaction. Metal NPs can serve as electron relay from electron donor BH_4^- ions (reductant) to the acceptor 4-nitrophenolate (oxidant) ions, overcoming the kinetic barrier and efficiently catalyse the reduction of 4-Nip to 4-Amp.[54] A typical UV-vis spectrum of 4-Nipaqueous solution shows a distinct absorption maximum peak at ~317 nm. Upon the addition of $NaBH_4$, the light yellow colour of 4-Nip changes to yellow-green and the 4-Nip peak is immediately red-shifted to 400 nm, due to the formation of 4-nitrophenolate ions in the alkaline medium caused by $NaBH_4$. The progress of the catalytic reaction was evaluated quantitatively by monitoring the changes of the absorption spectra of 4-nitrophenolate ions as a function of time after adding each of the SiO_2@Ag colloidal systems into the 4-Nip/$NaBH_4$ reaction mixture.[53]

As a control experiment, the catalytic activity of bare SiO_2 particles instead of SiO_2@Ag was evaluated. After a time period of six hours, no change of the nitrophenolate anions peak intensity was observed confirming the catalytic role of Ag NPs. However, after the addition of SiO_2@Ag nanocolloids, the reduction of 4-Nip by $NaBH_4$ and its conversion to 4-Amp was observed. Accordingly, the intensity of the peak at 400 nm gradually dropped with time accompanied by a concomitant appearance of a new peak at 295 nm indicating the formation 4-Amp. The UV-vis spectra were recorded at regular intervals of 50 seconds and they are depicted in Figure 8.Figure 8A represents the time dependent UV-vis spectra using theSiO_2@Ag-seed system as the reaction catalyst. The data imply that the reaction terminates within a time frame of 500 s consistent with the disappearance of the yellow colour of 4-Nip at the end of the reaction. Figure 8B and 8C display the time dependent reduction of 4-Nip using SiO_2@Ag-1 and SiO_2@Ag-2 particles, respectively. The results indicate that SiO_2@Ag-1 and SiO_2@Ag-2 systems effectively catalyse the reaction as well, however, at different reaction times. From the spectra presented in Figure 8A, 8B and 8C, it can be concluded that the intensity of the peak at 400 nm decreases gradually during the catalytic reaction but with a different reaction rate. Figure 8C demonstrates that, SiO_2@Ag-2 system requires the shortest time for the complete conversion of 4-Nip to 4-Amp. Consequently, the order of catalytic activity for the three different samples is *SiO_2@Ag-2>SiO_2@Ag-1>SiO_2@Ag-seed* and this trend is in accordance with the Ag nanoparticle size. Since the concentration of $NaBH_4$ greatly exceeds that of 4-Nip and SiO_2@Ag, the reduction rates can be assumed to be dependent only on the concentration of 4-Nip and independent of the $NaBH_4$ concentration. Taking into account the aforementioned assumption, the catalytic reaction rate constants (K) can be evaluated by studying the pseudo-first-order kinetics with respect to 4-Nip concentration.[55] As a result, the reaction rate constants (K) were calculated from the corresponding slopes, which can be determined from the linear fits of the $\ln(A_t/A_0)$ versus t plots. This allows the quantitative comparison of the catalytic activity of the three different nanocolloids as well as with other systems reported in literature, in which Ag-based nanocatalysts have been used in the reduction of 4-Nip. Specifically, A_t stands for absorbance at time t and A_0 for absorbance at time 0 which was taken as the time at 50 s corresponding to the second absorbance peak at 400 nm, because of the relatively small induction times (will be discussed in the next paragraph), observed at the beginning of each reaction.[53] Figure 8D demonstrates the reaction rate constants for the three different SiO_2@Ag systems, while all the plots present a good linear relation between $\ln(A_t/A_0)$ and time t, for almost 90% of the catalytic reactions. K exhibits the highest value for the

SiO_2@Ag-2 particles (K = 9.32±1.35×10^{-3} s^{-1}), whereas the lowest value was found for the SiO_2@Ag-seed system with a reaction rate constant of 2.91±0.21×10^{-3} s^{-1}. The results of the rate constants (K) are summarized in Table 1. In specific, it is worth to mention that the rate constant of the SiO_2@Ag-2 system found to be 9.32×10^{-3} s^{-1} is higher than values reported by Zhang (5.63×10^{-3} s^{-1}), Gangula (9.19×10^{-3} s^{-1}) and Huang (4.73×10^{-4} s^{-1}) et al.[53, 54, 56]

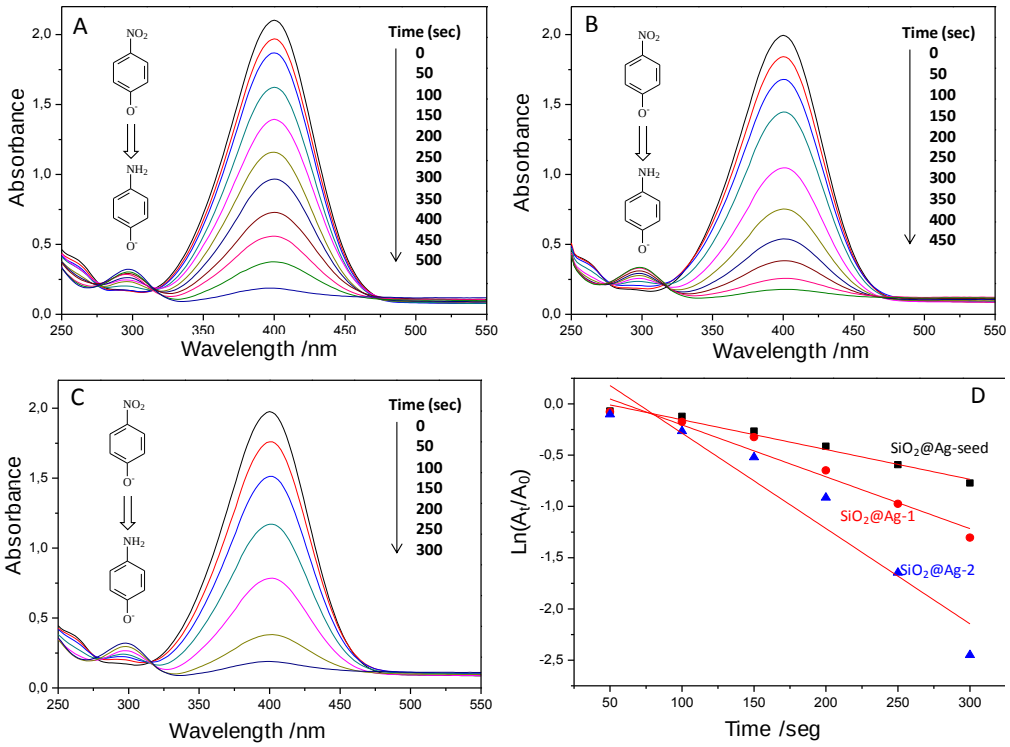

Figure 8. Time dependent UV-vis spectra (A, B and C) for the catalytic reduction of 4-Nip by $NaBH_4$ in the presence of SiO_2@Ag-seed, SiO_2@Ag-1 and SiO_2@Ag-2, respectively. D) Comparative plots of ln(A_t/A_0) versus time t towards the reduction reaction using SiO_2@Ag catalytic systems.

Table 1. Summary of the catalytic activity of the three different SiO_2@Ag systems towards the reduction of 4-Nip to 4-Amp by $NaBH_4$ at room temperature (20 °C).

Sample ID	Amount of SiO_2@Ag used (mg)	Aver. size of Ag NPs	Time of completion the reaction (s)	Calculated rate constant, K ($x10^{-3}s^{-1}$)
SiO_2@Ag-seed	0.5	4.2 ± 1.1	500	2.91±0.21
SiO_2@Ag-1	0.5	12.8 ± 3.4	450	5.06±0.51
SiO_2@Ag-2	0.5	18.6 ± 3.9	300	9.32±1.35

The induction time which was previously mentioned is a typical phenomenon for the heterogeneous catalysis, and related to the time required for the catalyst activation. In the reactions performed in our study, after addition of all the reactants, within the second spectrum run at a time interval of 50 s the absorbance intensity was already decreased revealing the initiation of the catalytic reaction. This observation can prove that the induction time in our systems was very small because the Ag NPs are directly in contact with the reaction components and no time for the diffusion of 4-Nip to reach the surface of meal NPs was needed like in other studies.[55, 57]Bigger induction times are normally attributed to many factors: *(i)* the diffusion-controlled adsorption of reactants onto the nanoparticle surface as already mentioned, *(ii)* the presence of dissolved oxygen in water reacting at a faster rate with $NaBH_4$ than with 4-Nip, *(iii)* the coating of a metal oxide layer onto the metal surface upon the addition of BH_4^-, poisoning the catalyst surface and *(iv)* a slow surface restructuring of the nanoparticles.[56]However, in our work the aqueous reaction medium containing the 4-Nip was degassed before adding the $NaBH_4$, therefore, we avoided the formation of an oxide layer at the Ag NP surface as well as the reaction of $NaBH_4$ with dissolved oxygen.

4. Conclusions

In summary, a relatively simple and facile method for the decoration of SiO_2 spheres with Ag NPs of tunable and uniform metal size has been developed. The general process involves the functionalization of SiO_2 particles with terminal amine groups and the coordination of silver ions which were reduced to Ag seeds. By using the SiO_2@Ag-seed system as a template, subsequent Ag growth steps were performed and the size of Ag seeds was remarkably increased, facilitating enhanced SERS and catalytic properties. The SERS ability can be exploited for the detection of conventional SERS analytes in water due to the long-term colloidal stability of all fabricated systems in aqueous media. It should be also emphasized that due to the limited use of organic solvents and toxic substances during the

synthetic process, this protocol can be defined in general as an environmentally 'green' synthetic approach, feasible to be scaled up for the production of bigger amounts of the hybrid particles.

Acknowledgements

This work was partly funded by the "POCO" European Project (NMP-213939) and the German Research Foundation (DFG) within the DFG-NSF cooperation project (DFG-Proj. Nr STA 324149-1) in the framework of 'Materials World Network'. The authors would like to thank Dr M. Malanin and Mrs A. Caspari for conducting the FT-IR and the zeta-potential measurements, respectively.

Notes and references

[a] Leibniz-Institut für Polymerforschung Dresden e.V., Hohe Straße 6, 01069 Dresden, Germany

[b] Technische Universität Dresden, Physical Chemistry of Polymer Materials, 01062 Dresden, Germany

[c] Department of Chemistry, University of Houston, Houston, Texas 77204, United States

1. M. A. El-Sayed, *Accounts of Chemical Research*, 2001, **34**, 257-264.
2. A. P. Alivisatos, *The Journal of Physical Chemistry*, 1996, **100**, 13226-13239.
3. U. V. Kreibig, M. , *Springer Series in Material Science.*, 1995, **Vol 25**.
4. S. Link and M. A. El-Sayed, *International Reviews in Physical Chemistry*, 2000, **19**, 409-453.
5. G. Mie, *Ann. Phys.*, 1908, **25**, 377-445.
6. M. Moskovits, *Reviews of Modern Physics*, 1985, **57**, 783-826.
7. T. Vo-Dinh, *TrAC Trends in Analytical Chemistry*, 1998, **17**, 557-582.
8. R. Contreras-Cáceres, S. Abalde-Cela, P. Guardia-Girós, A. Fernández-Barbero, J. Pérez-Juste, R. A. Alvarez-Puebla and L. M. Liz-Marzán, *Langmuir*, 2011, **27**, 4520-4525.
9. E. Hutter and J. H. Fendler, *Advanced Materials*, 2004, **16**, 1685-1706.
10. S. K. Ghosh and T. Pal, *Chemical Reviews*, 2007, **107**, 4797-4862.
11. H. Liu and Q. Yang, *Journal of Materials Chemistry*, 2011, **21**, 11961-11967.
12. M. Fleischmann, P. J. Hendra and A. J. McQuillan, *Chemical Physics Letters*, 1974, **26**, 163-166.
13. P. B. Johnson and R. W. Christy, *Physical Review B*, 1972, **6**, 4370-4379.
14. P. B. Johnson and R. W. Christy, *Physical Review B*, 1975, **11**, 1315-1323.
15. P. Herves, M. Perez-Lorenzo, L. M. Liz-Marzan, J. Dzubiella, Y. Lu and M. Ballauff, *Chemical Society Reviews*, 2012, **41**, 5577-5587.
16. D. D. Evanoff and G. Chumanov, *ChemPhysChem*, 2005, **6**, 1221-1231.
17. J. A. Creighton, C. G. Blatchford and M. G. Albrecht, *Journal of the Chemical Society, Faraday Transactions 2: Molecular and Chemical Physics*, 1979, **75**, 790-798.
18. P. C. Lee and D. Meisel, *The Journal of Physical Chemistry*, 1982, **86**, 3391-3395.
19. I. Pastoriza-Santos and L. M. Liz-Marzán, *Langmuir*, 1999, **15**, 948-951.
20. V. Bastys, I. Pastoriza-Santos, B. Rodríguez-González, R. Vaisnoras and L. M. Liz-Marzán, *Advanced Functional Materials*, 2006, **16**, 766-773.
21. T. C. Wang, M. F. Rubner and R. E. Cohen, *Langmuir*, 2002, **18**, 3370-3375.
22. Y. P. Zhao, D. X. Ye, G. C. Wang and T. M. Lu, *Nano Letters*, 2002, **2**, 351-354.
23. F. Mafuné, J.-y. Kohno, Y. Takeda, T. Kondow and H. Sawabe, *The Journal of Physical Chemistry B*, 2000, **104**, 8333-8337.
24. J. Zhu, S. Liu, O. Palchik, Y. Koltypin and A. Gedanken, *Langmuir*, 2000, **16**, 6396-6399.
25. N. A. Kotov, M. E. D. Zaniquelli, F. C. Meldrum and J. H. Fendler, *Langmuir*, 1993, **9**, 3710-3716.
26. S. Gupta, P. Uhlmann, M. Agrawal, S. Chapuis, U. Oertel and M. Stamm, *Macromolecules*, 2008, **41**, 2874-2879.
27. Z. Liu, X. Wang, H. Wu and C. Li, *Journal of Colloid and Interface Science*, 2005, **287**, 604-611.
28. C.-W. Chen, T. Serizawa and M. Akashi, *Langmuir*, 1999, **15**, 7998-8006.
29. Y. Lu, Y. Mei, M. Drechsler and M. Ballauff, *Angewandte Chemie International Edition*, 2006, **45**, 813-816.
30. S. Gupta, M. Agrawal, M. Conrad, N. A. Hutter, P. Olk, F. Simon, L. M. Eng, M. Stamm and R. Jordan, *Advanced Functional Materials*, 2010, **20**, 1756-1761.
31. R. Contreras-Caceres, C. Dawson, P. Formanek, D. Fischer, F. Simon, A. Janke, P. Uhlmann and M. Stamm, *Chemistry of Materials*, 2012, **25**, 158-169.
32. J. Li, C.-y. Liu and Y. Liu, *Journal of Materials Chemistry*, 2012, **22**, 8426-8430.
33. Z.-J. Jiang, C.-Y. Liu and L.-W. Sun, *The Journal of Physical Chemistry B*, 2005, **109**, 1730-1735.
34. C. Tian, B. Mao, E. Wang, Z. Kang, Y. Song, C. Wang and S. Li, *The Journal of Physical Chemistry C*, 2007, **111**, 3651-3657.
35. Q. Ji, J. P. Hill and K. Ariga, *Journal of Materials Chemistry A*, 2013, **1**, 3600-3606.
36. Z. Deng, M. Chen and L. Wu, *The Journal of Physical Chemistry C*, 2007, **111**, 11692-11698.
37. M. Zhu, G. Qian, Z. Hong, Z. Wang, X. Fan and M. Wang, *Journal of Physics and Chemistry of Solids*, 2005, **66**, 748-752.
38. Y. Kobayashi, V. Salgueiriño-Maceira and L. M. Liz-Marzán, *Chemistry of Materials*, 2001, **13**, 1630-1633.
39. W. Stöber, A. Fink and E. Bohn, *Journal of Colloid and Interface Science*, 1968, **26**, 62-69.
40. Y. An, M. Chen, Q. Xue and W. Liu, *Journal of Colloid and Interface Science*, 2007, **311**, 507-513.
41. S. Kobayashi, K. Hiroishi, M. Tokunoh and T. Saegusa, *Macromolecules*, 1987, **20**, 1496-1500.
42. Z. Yang, Y.-W. Lin, W.-L. Tseng and H.-T. Chang, *Journal of Materials Chemistry*, 2005, **15**, 2450-2454.
43. U. Kalapathy, A. Proctor and J. Shultz, *Bioresource Technology*, 2000, **73**, 257-262.
44. X. Lu and Y. Mi, *Macromolecules*, 2005, **38**, 839-843.
45. S. Sanchez-Cortes, R. M. Berenguel, A. Madejón and M. Pérez-Méndez, *Biomacromolecules*, 2002, **3**, 655-660.
46. V. Nerapusri, J. L. Keddie, B. Vincent and I. A. Bushnak, *Langmuir*, 2006, **22**, 5036-5041.
47. J. Rodríguez-Fernández, J. Pérez-Juste, F. J. García de Abajo and L. M. Liz-Marzán, *Langmuir*, 2006, **22**, 7007-7010.
48. T.-H. Liou, F.-W. Chang and J.-J. Lo, *Industrial & Engineering Chemistry Research*, 1997, **36**, 568-573.
49. P. Hildebrandt and M. Stockburger, *The Journal of Physical Chemistry*, 1984, **88**, 5935-5944.
50. V. Joseph, A. Matschulat, J. Polte, S. Rolf, F. Emmerling and J. Kneipp, *Journal of Raman Spectroscopy*, 2011, **42**, 1736-1742.
51. K. Kim and J. K. Yoon, *The Journal of Physical Chemistry B*, 2005, **109**, 20731-20736.
52. K. H. Su, Q. H. Wei, X. Zhang, J. J. Mock, D. R. Smith and S. Schultz, *Nano Letters*, 2003, **3**, 1087-1090.
53. W. Zhang, F. Tan, W. Wang, X. Qiu, X. Qiao and J. Chen, *Journal of Hazardous Materials*, 2012, **217–218**, 36-42.
54. A. Gangula, R. Podila, R. M, L. Karanam, C. Janardhana and A. M. Rao, *Langmuir*, 2011, **27**, 15268-15274.
55. A. M. Signori, K. d. O. Santos, R. Eising, B. L. Albuquerque, F. C. Giacomelli and J. B. Domingos, *Langmuir*, 2010, **26**, 17772-17779.
56. X. Huang, Y. Xiao, W. Zhang and M. Lang, *Applied Surface Science*, 2012, **258**, 2655-2660.
57. J. Yuan, S. Wunder, F. Warmuth and Y. Lu, *Polymer*, 2012, **53**, 43-49.

